Research Article | Vol. 31, No. 12 / 5 Jun 2023 / Optics Express 18790
Optics EXPRESS

Atmospheric dispersion management in mid-IR mode-locked oscillators

Evgeni Sorokin,[1,*] Alexander Rudenkov,[2] Nikolai Tolstik,[2] Vladimir Kalashnikov,[2] Maksim Demesh,[2] and Irina T. Sorokina[2]

[1] Photonics Institute, Vienna University of Technology, 1040 Vienna, Austria
[2] Department of Physics, Norwegian University of Science and Technology, N-7491 Trondheim, Norway
[*] evgenisorokin@tuwien.ac.at

Abstract: The atmospheric dispersion in the mid-infrared transparency windows presents an important albeit often neglected factor when developing ultrashort-pulsed lasers. We show that it can amount to hundreds of fs^2 in 2–3 μm window with typical laser round-trip path lengths. Using the Cr:ZnS ultrashort-pulsed laser as a test-bed, we demonstrate the atmospheric dispersion influence on femtosecond and chirped-pulse oscillator performance and show that the humidity fluctuations can be compensated by an active dispersion control, greatly improving stability of mid-IR few-optical cycle laser sources. The approach can be readily extended to any ultrafast source in the mid-IR transparency windows.

1. Introduction

The mid-infrared (mid-IR) wavelength range, broadly defined as the range between roughly 2 and 20 μm [1] is also often called a "molecular fingerprint" region. Ultrafast sources in this wavelength region may be attractive for many applications such as sensing, bio-medicine, material processing, and science. A large progress has been made in the last decade for crystalline lasers, most notably Cr:ZnSe and Cr:ZnS [2–4]. Its operation range between 2 and 3 μm is characterized by the presence of the strong fundamental and overtone vibrational absorption lines of atmospheric constituents. Those include water vapour (H2O), having the maximum around 2.6–2.7 μm, carbon monoxide (CO) with strong features around 2.3–2.4 μm, methane, carbon dioxide, nitrous oxide (N2O) and others. This spectral overlap also makes the sources prone to the adverse influence of these very molecules when they appear in the atmosphere.

For broader usage the mid-IR lasers have to be convenient in handling, not overly expensive and, most importantly, provide stable and reliable operation, be it a supercontinuum source [5,6], frequency comb [7,8], spectroscopic instrument [9,10], or a seed for further amplification [11–13]. This is, however, confronted by the observed dependence of device parameters on atmospheric conditions, in particular the humidity, which can vary quite strongly. Complete evacuation of the sources could solve the problem at a cost of price, size, and user unfriendliness. It is important therefore to characterize and be able to counteract the influence of the naturally changing atmosphere on the operation parameters of such sources, opening way to self-adjusting "smart laser" solid-state oscillator design in the mid-IR [14,15].

2. Air dispersion

Before proceeding we must note that an ultrafast laser oscillator is quite stable against the losses, introduced by the narrow absorption lines of the molecular gases. The direct influence of the narrow absorption lines has been observed and well understood [16–19] to cause only additional narrowband peaks on the spectrum, which hardly affect the pulse itself. The purpose of this work is to study the influence of dispersion, associated with the absorption lines.

#488683 https://doi.org/10.1364/OE.488683
Journal © 2023 Received 1 Mar 2023; revised 28 Apr 2023; accepted 28 Apr 2023; published 22 May 2023

Optics EXPRESS

There exist many experimental techniques to assess the dispersion, which include direct measurement of the group delay in the time domain and interferometric techniques in the frequency domain. These techniques experience difficulties when the measured materials exhibit strong absorption, and since calculation of the second-order dispersion involves differentiation, low and hence noisy signal results in the very high uncertainty of the result.

Another way of dispersion calculation is to use the Kramers-Kronig relation from the known absorption data of the atmosphere constituents, which can be taken from e.g., HITRAN database [20–22]. The narrow rovibrational absorption lines are represented there by the Voigt contour, which is a convolution of the pressure broadening (Lorentzian) and Doppler broadening (Gaussian). Summing contributions from all lines provides the absorption spectrum in a very broad range from the UV to the far infrared for any given atmosphere composition, temperature and pressure. Taking this spectrum in the frequency domain as the imaginary part of the complex index of refraction allows calculating its real part from absorption coefficient $\alpha(\omega)$:

$$n(\omega) = 1 + \frac{c}{\pi} v.p. \int \frac{\alpha(\omega')}{\omega'^2 - \omega^2} d\omega'. \tag{1}$$

The propagation constant $\beta(\omega) = \omega n(\omega)/c$ can then be numerically differentiated to obtain the group velocity dispersion (GVD) $\beta_2 = d^2\beta(\omega)/d\omega^2$. At normal atmospheric conditions, where the pressure broadening dominates, a standard procedure is to use Lorentzian shapes, where analytical expressions can be used to simplify calculations [23].

Direct calculation according to expression (1) for gases results in a wildly oscillating GVD curve (Fig. 1(a)). This is because the second derivative of the narrow line with characteristic width $\Delta\omega$ scales as $\Delta\omega^{-2}$ and for the typical width of the atmospheric lines at normal condition of ~0.1 cm^{-1} even a weak absorption line produces oscillations with ps^2/m amplitude and more. For the ultrashort pulse propagation this kind of GVD is not relevant, because physically the narrow absorption feature only results in a long tail (free induction decay) behind the pulse with duration $\sim\Delta\omega^{-1}$ being many tens of picoseconds long and its overlap with the pulse is negligible. However, each absorption line does contribute to a slowly varying refractive index curve far beyond the line width, which will result in a GVD. It becomes necessary to correctly remove the narrowband features from the calculated curve in Fig. 1(a).

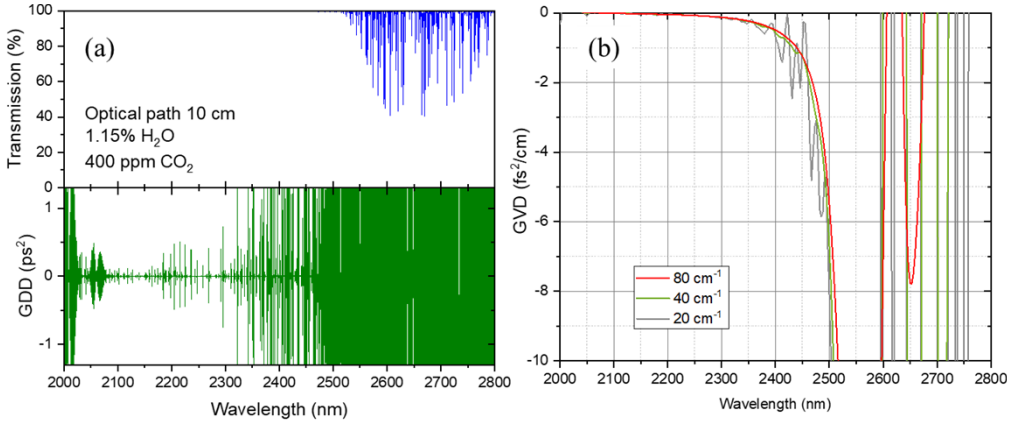

Fig. 1. (a) Transmission of the atmosphere and corresponding GDD for the 10 cm optical path at 40% relative humidity (r.h.) at $T = 296$ K and $p = 1$ atm. Note the scale of the GDD, which is in picoseconds squared. (b) Example of the GVD data processed by windowing out absorption lines around the measurement point with different width of the excluding window.

Optics EXPRESS

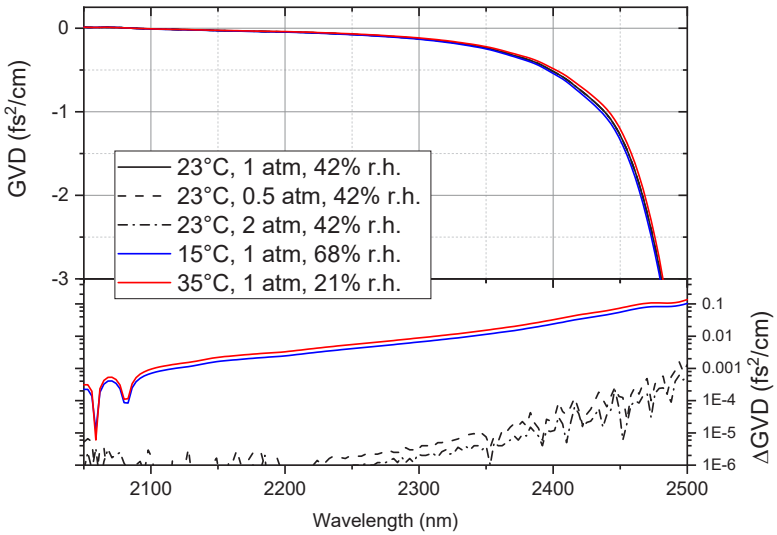

Fig. 2. Dispersion variation with pressure and temperature. The lower tab shows the absolute deviation of dispersion compared to that for 296 K, 1 atm. All data has been calculated for 1.15% water vapour content and scaled to the same absolute concentration of $2.85 \cdot 10^{17}\mathrm{cm}^{-3}$ (41.5% r.h. at 296 K and 1 atm. pressure).

We have tested and compared few approaches to separate the narrow-band oscillations and the slowly varying part of the GVD: brute-force smoothing of the GVD curve, windowing out the absorption lines around the measurement point (Fig. 1(b)), and exclusion of the absorption line central area. We have also simulated some time-domain measurement schemes, such as a white-light interferometer, asymmetric second order autocorrelator, as well as group delay of a probe pulse.

The details of these procedures are described in Supplemental materials, here we will only summarize the common features. First, all methods provide compatible results in the transparency windows, where only few weak absorption lines are present, while differing in the areas with many densely located absorption lines, such as e.g., water vapour band around 2.7 μm. Second, the results critically depend on the spectral width parameter: window width for the smoothing, pulse spectral width for the white-light interferometer, autocorrelator and group delay calculation, and the width of the excluded area for the windowing or the line center exclusion techniques. Too narrow width results in residual modulation of the dispersion function, while processing with excessive width would decrease the resolution and incur the influence of the strong absorption bands onto the transparent regions. In the rest of the paper, we show the dispersion data obtained using the $60\,\mathrm{cm}^{-1}$ super-Gaussian excluding window procedure, which provided smooth dispersion at reasonable spectral resolution. The effective dispersion within the dense absoption bands, where different smoothing procedures provide conflicting results requires separate investigation and experimental confirmation.

For practical use, one should also establish the dependence of dispersion on the atmosphere parameters. It follows from the basic principles, that the real part of the refractive index, associated with a narrow absorption line at ω_0, has broad wings which decay asymptotically as $(\omega_0 - \omega)^{-1}$ [24]:

$$n(\omega) \approx 1 + \frac{c}{2\pi\omega_0(\omega_0 - \omega)} \int \alpha(\omega')d\omega'. \tag{2}$$

Validity of this approximation can be easily seen analytically for the Lorentzian lineshape, but the expression is more general since the integral is independent of the exact shape and broadening

Optics EXPRESS

factor of the absorption line. Thus, the contribution of a line to the slowly varying dispersion does not depend directly on pressure or temperature, but only on its integral cross-section and the volume concentration of absorbing molecules in the atmosphere. Also, if the temperature is within the normal laboratory ranges, the cross-section distribution of the rotational components does not vary much and can be taken at HITRAN reference temperature of 296 K (Fig. 2). This allows using the tabulated GVD results for normal conditions, just scaled by the volume concentration of the absorbing molecules. We provide datasets for separate calculation of dispersion due to water vapour and carbon dioxide in Supplement 1.

3. Experimental verification

To verify our model calculation we have constructed a Kerr-lens modelocked (KLM) ultrashort-pulse oscillator based on a Cr:ZnS laser (Fig. 3), with pulse repetition rate 69 MHz and round-trip air path L = 433 cm. We have detailed dispersion data of all materials and of all mirrors. The mirror group delay dispersion (GDD) can be calculated from the coating design, but to allow for the layer thickness error during manufacturing, the layer thicknesses have been corrected by refining the design using the measured transmission curve. The YAG wedges allowed fine and controllable adjustment of the GDD. Detailed dispersion data are provided in Supplement 1.

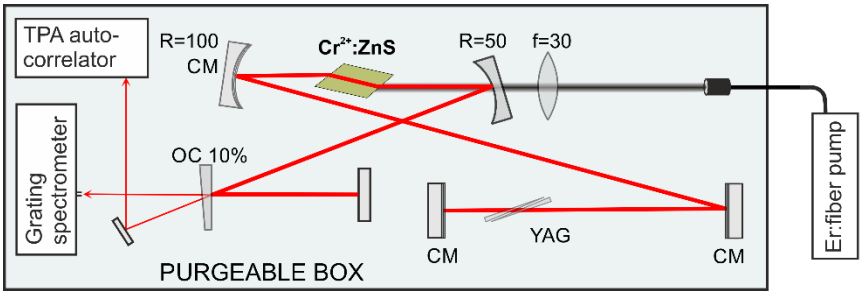

Fig. 3. Experimental setup. CM: the high reflecting mirrors which could be substituted for chirped mirrors. OC: output coupler. YAG: a Brewster pair of the 3° YAG wedges. The wedge insertion was measured along one of the wedges, with 25 and 0 mm insertion corresponding to 1.6 and 3.2 mm of combined wedge thickness, respectively.

The oscillator has been adjusted to operate in the vicinity of the zero GDD so that it was possible to switch the round-trip GDD from normal to anomalous by changing the wedge insertion or adding a calcium fluoride Brewster plate. With anomalous round-trip GDD the laser operated in the femtosecond regime with pulse duration τ = 30–60 fs and 150–300 nm spectral width at half-maximum. With the normal round-trip GDD the laser operated as a chirped-pulse oscillator (CPO [25], also called dissipative soliton in the literature [26]) with τ = 0.7–2 ps and 120–180 nm spectral width. To exclude thermal effects, we operated the oscillator at relatively low output power of 100 mW per OC bounce, corresponding to 14.4 nJ intracavity energy at 69 MHz repetition rate, and used temperature stabilization of the active medium. Since both the soliton and CPO regimes are subject to respective area theorems [27,28] connecting their duration and energy, we made sure to maintain exactly the same intracavity energy in every data series.

To control the atmosphere, the laser has been put in a box, which was purged with dry nitrogen, with the grating spectrometer (WaveScan by APE) and a home-made collinear two-photon absorption (TPA) autocorrelator inside the box. We could continuously measure the humidity inside the box, however, we found that this was a very inaccurate measurement. The humidity sensor was quite slow and measured the humidity only at its own position in the box. We therefore assessed the water vapour concentration by measuring the relative amplitude of the feature at

Optics EXPRESS

2435 nm on a soliton spectrum, which is proportional to the total absorption of the corresponding water line [16]. This is much more relevant data, as it is immediate and shows the average water molecule concentration along the actual beam path (see Supplement 1 for details).

3.1. Soliton regime

To obtain the possibly short pulses one would strive to provide small negative GDD over the whole expected range. Consequently, the oscillator becomes quite sensitive to the dispersion changes due to the humidity fluctuations. As an example, in Fig. 4 the atmosphere at open air keeps the GDD modulation peak from the chirped mirrors low. With dry nitrogen purging the peak at 2350 nm goes above zero, and the pulse spectrum starts to develop a double-headed shape, typical for the fourth-order dominated intracavity dispersion [29].

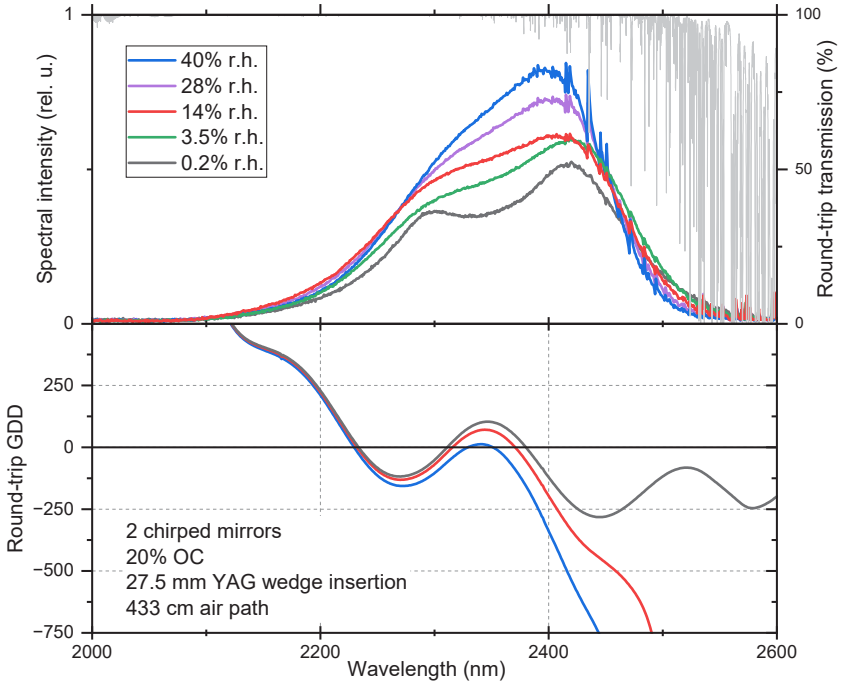

Fig. 4. Effect of humidity change on short-pulse oscillator spectrum. The GDD curves differ only by the amount of the himidity-related dispersion. The oscillator had a combination of mirrors as in Fig. 2 except a 20% output coupler instead of two bounces from a 10% OC. The round-trip atmospheric transmission (gray curve) is calculated for 40% r.h. at 296 K and 1 atm at full spectral resolution.

Adding a 3 mm CaF_2 Brewster plate and removing one CM bounce turns the oscillator to a longer-pulse regime with τ = 50–55 fs and strong dispersive-wave feature at 2060 nm due to the uncompensated third-order dispersion (TOD). In this regime, complete purging the box results in just a shift of the spectrum towards the longer wavelengths by 25 nm (Fig. 5(a)). This setup is characterized by the dominating TOD, so that the additional atmospheric dispersion does not introduce any significant qualitative change. The laser operates in a nearly chirp-free regime with $\Delta\nu\Delta\tau \sim 0.35$. The small residual chirp (Fig. 5(b)) is due to the uncompensated 640 fs^2 dispersion of the 3-mm output coupler on a fused silica substrate. It is worth noting, that the additional losses, introduced to the pulse by absorption in the atmosphere (gray line in Fig. 5) amount to only 0.5% at 38% r.h. as compared to 20% OC output coupler transmission, proving that in this case the absorption losses are all but negligible perturbing factor.

Optics EXPRESS

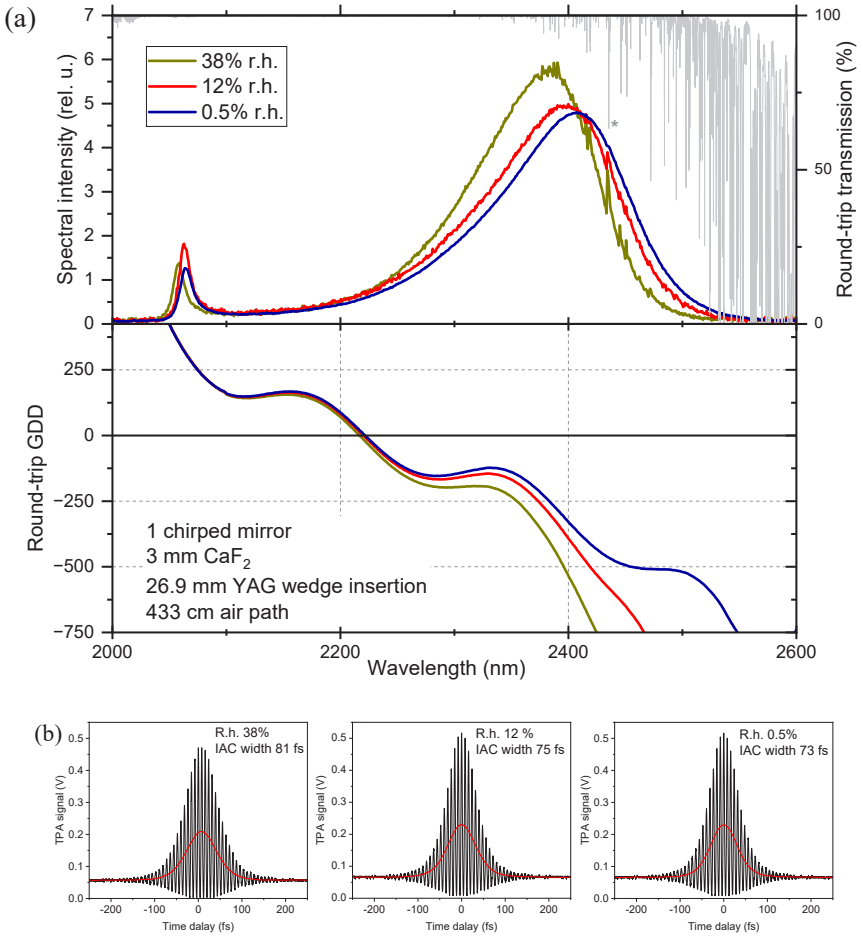

Fig. 5. (a) Spectra and GDD of the long-pulse oscillator setup. The GDD curves differ only by the amount of the himidity-related dispersion. The round-trip atmospheric transmission (gray curve) is calculated for 38% r.h. at 296 K and 1 atm at full spectral resolution. The gray star marks the water absorption line at 2435 nm, which was used as a humidity sensor. (b) Autocorrelation traces for the output pulses. IAC: intensity autocorrelation (red line).

3.2. *CPO regime*

The chirped-pulse regime in solid-state lasers is known to be very sensitive to dispersion [30] and even very small changes result in the visible deformation of the spectrum. In addition to that, the CPO spectrum is cut at the edges, so that it interacts only with a limited and clearly identifiable range of the GDD curve. In our setup, this range was well in the water-free window so that there were no additional sources of losses at the wings. The typical behavior of a CPO oscillator under purging is shown in Fig. 6(a).

At the same time, changing the insertion of the YAG wedges also changes the GDD, as shown in Fig. 6(b). By manipulating the wedge insertion and purging it is possible to approximately compensate both effects, so that the spectra and autocorrelations become nearly identical for the same pulse enrgy (Fig. 6(c)). As one can see from the GDD curves, the dispersion increase due to the wedges insertion nearly compensates (in the first order) the atmospheric GDD decrease due to the purging. This as a direct experimental confirmation for dispersion calculation procedure, allowing one to design a humidity compensator, that would use the independent humidity,

Optics EXPRESS

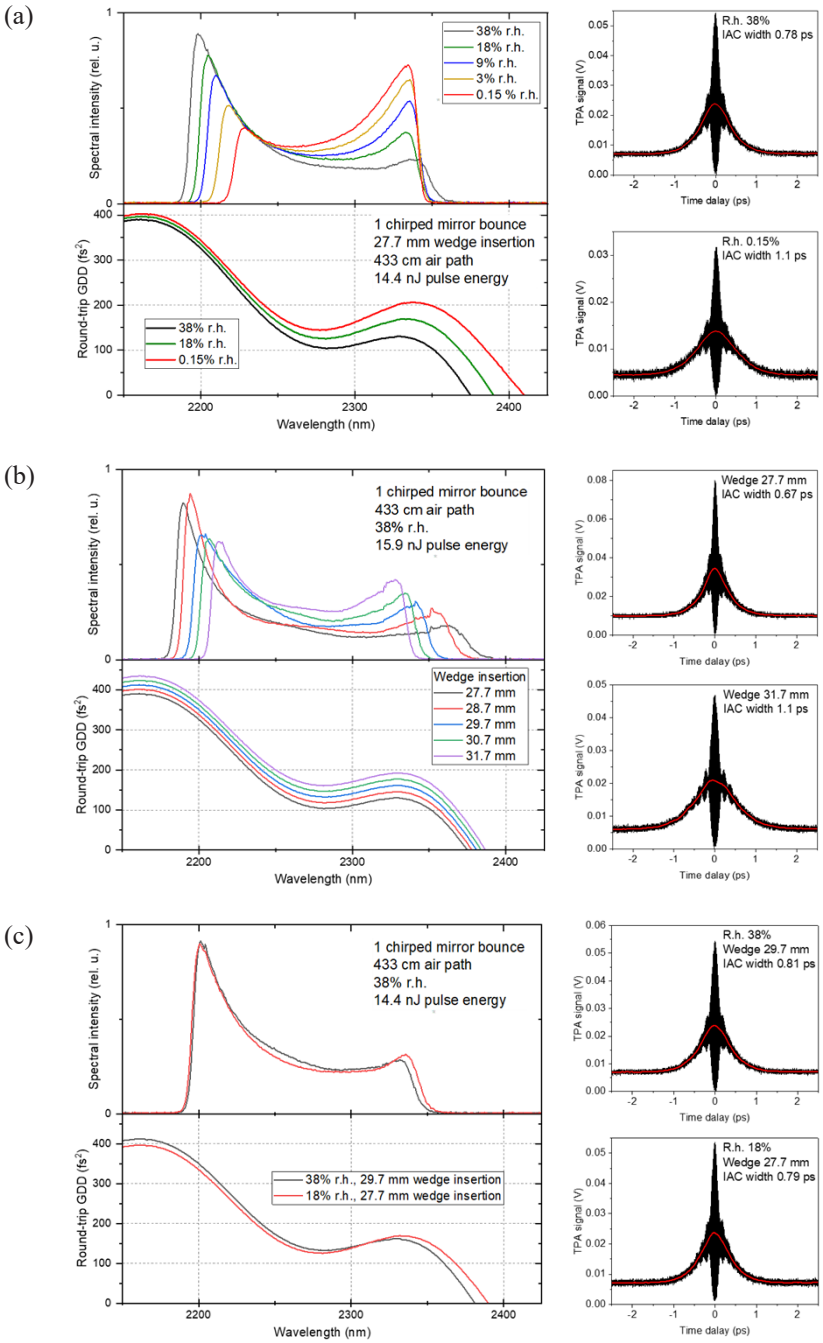

Fig. 6. (a) CPO oscillator spectra and autocorrelation traces under nitrogen purging. (b) CPO oscillator spectra and autocorrelation traces at open air with different YAG wedge insertions. (c) Approximate compensation of higher humidity by increased YAG wedge insertion. For all graphs, the lower plot shows the round-trip GDD, which includes the himidity-related dispersion calculated for the given r.h. level. Note that the intracavity pulse energy was different for (a) and (b) series.

Optics EXPRESS

temperature, and pressure gauges to control the dispersion in real time, thus greatly improving stability of the oscillator.

4. Conclusion

The atmospheric influence in the MID-IR is significant even in the nominally transparent wavelength regions. The reason is less absorption, but rather the dispersion influence, which is comparable to that of the net GDD of a typical oscillator, operating around 100 MHz repetition rate. From the atmospheric constituents, the air humidity makes the largest contribution in the wavelength range below 3.5 μm, while CO_2 dominates around its 4.2 μm absorption band. If complete evacuation is not desirable, it is possible to use the finely adjustable dispersive elements, such as wedge pairs, to compensate in the first order for atmospheric absorber concentration, pressure, and temperature fluctuations in the lab. The exact amount of required compensation can be calculated with the HITRAN data and used e.g., in an automated control scheme with separate gauges.

Funding. Norges Forskningsråd (303347, 326503).

Disclosures. The authors declare no conflicts of interest.

Data availability. Data underlying the results presented in this paper are not publicly available at this time but may be obtained from the authors upon reasonable request.

Supplemental document. See Supplement 1 for supporting content.

References

1. I. T. Sorokina, "Crystalline Mid-Infrared Lasers," in *Solid-State Mid-Infrared Laser Sources*, I. T. Sorokina and K. Vodopyanov, eds. (Springer, 2003), pp. 262–358.
2. I. T. Sorokina and E. Sorokin, "Femtosecond Cr^{2+}-based Lasers," IEEE J. Select. Topics Quantum Electron. **21**(1), 273–291 (2015).
3. S. B. Mirov, I. S. Moskalev, S. Vasilyev, V. Smolski, V. V. Fedorov, D. Martyshkin, J. Peppers, M. Mirov, A. Dergachev, and V. Gapontsev, "Frontiers of Mid-IR Lasers Based on Transition Metal Doped Chalcogenides," IEEE J. Select. Topics Quantum Electron. **24**(5), 1–29 (2018).
4. S. Qu, A. Paudel, A. Sebesta, P. Steinleitner, N. Nagl, M. Poetzlberger, V. Pervak, K. F. Mak, and A. Weigel, "Directly diode-pumped femtosecond Cr:ZnS amplifier with ultra-low intensity noise," Opt. Lett. **47**(23), 6217–6220 (2022).
5. S. Vasilyev, I. Moskalev, V. Smolski, J. Peppers, M. Mirov, A. Muraviev, K. Vodopyanov, S. Mirov, and V. Gapontsev, "Multi-octave visible to long-wave IR femtosecond continuum generated in Cr:ZnS-GaSe tandem," Opt. Express **27**(11), 16405–16412 (2019).
6. J. Zhang, K. Fai Mak, N. Nagl, M. Seidel, D. Bauer, D. Sutter, V. Pervak, F. Krausz, and O. Pronin, "Multi-mW, few-cycle mid-infrared continuum spanning from 500 to 2250 cm^{-1}," Light: Sci. Appl. **7**(2), 17180 (2017).
7. M. Kowalczyk, N. Nagl, P. Steinleitner, V. Pervak, A. Głuszek, J. Sotor, F. Krausz, A. Weigel, and K. F. Mak, "CEP-stable Single-Cycle Pulses from a Cr:ZnS Laser," in *Conference on Lasers and Electro-Optics*, Technical Digest Series (Optica Publishing Group, 2022), paper SF2E.4.
8. S. Vasilyev, I. Moskalev, V. Smolski, J. Peppers, M. Mirov, Y. Barnakov, V. Fedorov, D. Martyshkin, S. Mirov, and V. Gapontsev, "Kerr-lens mode-locked Cr:ZnS oscillator reaches the spectral span of an optical octave," Opt. Express **29**(2), 2458–2465 (2021).
9. E. Sorokin, I. T. Sorokina, J. Mandon, G. Guelachvili, and N. Picque, "Sensitive multiplex spectroscopy in the molecular fingerprint 2.4 μm region with a Cr^{2+}:ZnSe femtosecond laser," Opt. Express **15**(25), 16540–16545 (2007).
10. B. Bernhardt, E. Sorokin, P. Jacquet, R. Thon, T. Becker, I. T. Sorokina, N. Picqué, and T. W. Hänsch, "Mid-infrared dual-comb spectroscopy with 2.4 μm Cr^{2+}:ZnSe femtosecond lasers," Appl. Phys. B **100**(1), 3–8 (2010).
11. P. Fuertjes, L. von Grafenstein, C. Mei, M. Bock, U. Griebner, and T. Elsaesser, "Cr:ZnS-based soliton self-frequency shifted signal generation for a tunable sub-100 fs MWIR OPCPA," Opt. Express **30**(4), 5142–5150 (2022).
12. Y. Wu, F. Zhou, E. W. Larsen, F. Zhuang, Y. Yin, and Z. Chang, "Generation of few-cycle multi-millijoule 2.5 μm pulses from a single-stage Cr2+:ZnSe amplifier," Sci. Rep. **10**(1), 7775 (2020).
13. S.-H. Nam, G. C. Nagar, D. Dempsey, O. Novák, B. Shim, and K.-H. Hong, "Multi-octave-spanning supercontinuum generation through high-energy laser filaments in YAG and ZnSe pumped by a 2.4 μm femtosecond Cr:ZnSe laser," High Power Laser Sci. Eng. **9**, e12 (2021).
14. R. I. Woodward and E. J. R. Kelleher, "Towards 'smart lasers': self-optimisation of an ultrafast pulse source using a genetic algorithm," Sci. Rep. **6**(1), 37616 (2016).
15. T. Baumeister, S. L. Brunton, and J. Nathan Kutz, "Deep learning and model predictive control for self-tuning mode-locked lasers," J. Opt. Soc. Am. B **35**(3), 617–626 (2018).

Optics EXPRESS

16. V. L. Kalashnikov and E. Sorokin, "Soliton absorption spectroscopy," Phys. Rev. A **81**(3), 033840 (2010).
17. V. L. Kalashnikov, E. Sorokin, and I. T. Sorokina, "Chirped dissipative soliton absorption spectroscopy," Opt. Express **19**(18), 17480–17492 (2011).
18. D. Okazaki, W. Song, I. Morichika, and S. Ashihara, "Mode-locked laser oscillation with spectral peaks at molecular rovibrational transition lines," Opt. Lett. **47**(23), 6077–6080 (2022).
19. N. Nishizawa, S. Kitajima, and Y. Sakakibara, "Spectral peaking in an ultrashort-pulse fiber laser oscillator with a molecular gas cell," Opt. Lett. **47**(10), 2422–2425 (2022).
20. L. S. Rothman, D. Jacquemart, and A. Barbe, *et al.*, "The HITRAN 2004 molecular spectroscopic database," J. Quant. Spectrosc. Radiat. Transfer **96**(2), 139–204 (2005).
21. R. J. Mathar, "Refractive index of humid air in the infrared: model fits," J. Opt. A: Pure Appl. Opt. **9**(5), 470–476 (2007).
22. R. J. Mathar, "Calculated Refractivity of Water Vapor and Moist Air in the Atmospheric Window at 10 μm," Appl. Opt. **43**(4), 928–932 (2004).
23. A. A. Voronin and A. M. Zheltikov, "The generalized Sellmeier equation for air," Sci. Rep. **7**(1), 46111 (2017).
24. L. Landau, E. Lifshitz, and L. Pitaevskii, *Electrodynamics of continuous media*, Course of Theoretical Physics (Elsevier, 2013), Vol. 8.
25. A. Fernandez, T. Fuji, A. Poppe, A. Fürbach, F. Krausz, and A. Apolonski, "Chirped-pulse oscillators: a route to high-power femtosecond pulses without external amplification," Opt. Lett. **29**(12), 1366–1368 (2004).
26. P. Grelu and N. Akhmediev, "Dissipative solitons for mode-locked lasers," Nat. Photonics **6**(2), 84–92 (2012).
27. W. H. Renninger, A. Chong, and F. W. Wise, "Area theorem and energy quantization for dissipative optical solitons," J. Opt. Soc. Am. B **27**(10), 1978–1982 (2010).
28. G. P. Agrawal, *Nonlinear fiber optics*, 4th ed. (Academic, 2006).
29. I. P. Christov, M. M. Murnane, H. C. Kapteyn, J. Zhou, and C. P. Huang, "Fourth-order dispersion-limited solitary pulses," Opt. Lett. **19**(18), 1465–1467 (1994).
30. E. Sorokin, N. Tolstik, V. L. Kalashnikov, and I. T. Sorokina, "Chaotic chirped-pulse oscillators," Opt. Express **21**(24), 29567–29577 (2013).